Chem. Res. Chin. Univ., 2016, 32(3), 484—492 doi: 10.1007/s40242-016-5471-5

Synthesis and Gelation Capability of Fmoc and Boc Mono-substituted Cyclo(*L*-Lys-*L*-Lys)s

ZONG Qianying[1], GENG Huimin[1], YE Lin[1], ZHANG Aiying[1], SHAO Ziqiang[1,2] and FENG Zengguo[1*]

1. School of Materials Science and Engineering, Beijing Institute of Technology, Beijing 100081, P. R. China;
2. Beijing Engineering Research Center of Cellulose and Its Derivatives, Beijing 100081, P. R. China

Abstract Fmoc or Boc mono-substituted cyclo(*L*-Lys-*L*-Lys)s were synthesized *via* the reaction of lysine cyclic dipeptide with Fmoc *N*-hydroxysuccinimide este(Fmoc-OSu) and di-tert-butyl dicarbonate[$(Boc)_2O$], respectively. The resulted mono-substituted cyclo(*L*-Lys-*L*-Lys)s(**2—4**) by means of test tube inversion method served as organogelators enabled to form stable thermo-reversible organogels in alcoholic, substituted benzene and chlorinated solvents, with the minimum gelation concentration(MGC) in a range of 1%—4%(mass fraction). The transmission electron microscopy(TEM) and scanning electron microscopy(SEM) observations reveal that these gelators self-assembled into 3D nanofiber, nanoribbon or nanotube network structures. The rheological measurement exhibited that the storage modulus of gels is higher than the loss one, and the complex viscosity is reduced linearly with the increasing of scanning frequency. The fluorescence spectrum of compound **2** in 1,2-dichloroethane and benzene demonstrates that the emission peak of Fmoc at 320 nm has red-shifted and the intensity decreases gradually, while the intensity of the emission peak at 460 nm substantially enhances as a function of concentration, indicating the existence of π-π stacking interactions and the formation of J-type aggregates. Meanwhile, compound **4** self-assembled into nanotubes *via* the stacking of multiple bilayer membranes. Fmoc and Boc disubstituted cyclo(*L*-Lys-*L*-Lys)(**3**) holds the relatively lower MGC values, showing the stronger gelation ability in most selected organic solvents due to the presence of both Fmoc and Boc groups.

Keywords Lysine cyclic dipeptide; Low molecular weight gelator; π-π Stacking; Nanotube

1 Introduction

Like macromolecules, low-molecular-weight gelators (LMWGs) can also generate physical gels driven by non-covalent intermolecular forces, such as hydrogen bonding, π-π stacking, electrostatic interaction and so on. However, different from that of those classical polymeric gels, the gelation of LMWGs occurs *via* the three-dimensional(3D) self-assembled fibrillar polymeric networks constructed from the non-covalent interactions of gelators to entrap a vast amount of solvent molecules into the gels. The intrinsic supramolecular characters of these physical gels make them promising candidates used as emerging smart materials[1—5]. Cyclic dipeptides or 2,5-diketopiperazine(DKP) derivatives are the smallest cyclic peptide molecules, generally derived from the condensation of two α-amino acids with functionalized side chains. Some of them frequently occur in nature with a wide spectrum of biological activity. Recently, a lot of efforts have been devoted toward the synthesis of cyclic dipeptide derivatives and the gelation potential for organic solvents and water applied in the fields of spilt crude oil recovery, drug discovery, drug controlled delivery, etc.[6—9]. For example, cyclo(*L*-Tyr-*L*-Lys) was shown not only to possess antinociceptive activity[10], but also to gelate a number of polar organic solvents, such as dimethylsulfoxide(DMSO), dimethylacetamide(DMAC) and dimethylformamide(DMF), and even water under the assistance of ultrasound[11]. Gelators obtained from cyclo(*L*-Asp-*L*-Phe) can create thixotropic gels in ionic liquids[12,13]. Shear-assisted hydrogels with thixotropic character were also illustrated by simply applying a shear force to a metastable supersaturated solution of cyclo(*L*-Tyr-*L*-Lys) glycosylated derivative[14].

In a recent article, we reported that Fmoc and Boc disubstituted cyclo(*L*-Lys-*L*-Lys)s can give rise to stable organogels in selected alcoholic, substituted benzene and chlorinated solvents with the minimum gelation concentration(MGC) in a range of 1%—5%[15]. At the same time, a series of symmetrical peptidomimetics was synthesized from cysteine-modified cyclo (*L*-Lys-*L*-Lys)s and the corresponding gelation capability in organic solvents was also evaluated[16]. Furthermore, these peptidomimetics can selectively gelate chlorinated organic solvents in water if used as organogelators and can high efficiently adsorb a number of tested dyes from aqueous solutions if served as xerogels[17]. If the broad biological and pharmaceutical activity and robust gelation ability are taken into account, the synthesis and gelation assessment of hydrogelators based on cyclo(*L*-Lys-*L*-Lys)s is a part of our continuing

*Corresponding author. E-mail: sainfeng@bit.edu.cn
Received December 4, 2015; accepted March 11, 2016.
Supported by the National Natural Science Foundation of China(No.21174018).

research program on the chemistry of cyclic dipeptides[14—17]. However, the Fmoc, Boc and cysteine disubstituted lysine cyclic dipeptides are insoluble in water as LMWGs. To this end, three Fmoc and Boc mono-substituted cyclo(*L*-Lys-*L*-Lys)s (**2—4**) were synthesized and tested in this study. The synthesis is facile with high yield and no racemization. Fmoc mono-substituted lysine cyclic dipeptide(**2**) is slightly soluble in water to give access to partial hydrogel, showing promise as a platform to prepare hydrogelators. Meanwhile, Boc mono-substituted lysine cyclic dipeptide(**4**) is self-assembled into nanotubes by forming bilayer membrane(BLM) structures in most selected organic solvents. The supramolecular architectures of the resulted nanotubes with a well-defined hollow cylindrical morphology and precisely controlled dimension would open an avenue to a new phase of functional materials and biological or analytical application[18—20].

2 Experimental

2.1 Materials and Methods

Fmoc *N*-hydroxysuccinimide este(Fmoc-OSu) and di-tert-butyl dicarbonate[$(Boc)_2O$] were supplied by J&K Chemicals(China) and all other reagents were supplied by VAS Chemical Reagent Company, Tianjin, China. The starting material cyclo(*L*-Lys-*L*-Lys)·2HBr(**1**) was synthesized according to the literature[21—23]. ^{1}H nuclear magnetic resonance(^{1}H NMR) analyses were carried out on a Bruker AV-400 NMR spectrometer. Infrared(IR) spectra were recorded on a Shimadzu Trance-10 IR spectrometer. ESI-TOF MS analyses were conducted on a Bruker Autoflex mass spectrometer; transmission electron microscopy(TEM) images were obtained on a JEOL JEM-1200 microscope. Scanning electron microscopy(SEM) images were taken on an S-4800 Hitachi FE-SEM. Fluorescence spectrum was measured on a Varian Cary Eclipse spectrometer with the aid of excitation at 265 nm and emission data were ranged between 250 and 600 nm. Rheological measurement was performed on a strain-controlled Anton-Paar Physica MCR301 rheometer with the concentric cylinder geometry. X-Ray diffraction(XRD) patterns were obtained from a Philips X'Pert Pro MPD with Cu $K\alpha$(λ=0.15405 nm) radiation.

2.2 Synthesis of Fmoc-cyclo(*L*-Lys-*L*-Lys)-NH_2(2)

Cyclo(*L*-Lys-*L*-Lys)·2HBr(**1**, 1.255 g, 3.0 mmol) was dissolved together with $NaHCO_3$(8 mmol, 0.192 g) in 50 mL of H_2O, and the solution was slowly added in the solution of Fmoc-OSu(1.0 mmol, 0.337 g) dissolved in 50 mL of 1,4-dioxane at 0 °C. The reaction was warmed to room temperature and stirred overnight. The reaction mixture gradually turned turbid with a sub-transparent appearance. The solution was concentrated before washed with water, the precipitate was dissolved in 1 mol/L HCl, and the insoluble was discarded. Finally the target product was gathered by precipitating it with 1 mol/L NaOH, and freeze-dried, giving a white powder. Yield: 65%; m. p. 165 °C; ^{1}H NMR(400 MHz, DMSO-d_6, 25 °C), δ: 8.09(s, 2H), 7.88(d, *J*=7.3 Hz, 3H), 7.67(d, *J*=7.3 Hz, 1H), 7.40(t, *J*=7.2 Hz, 1H), 7.32(t, *J*=7.1 Hz, 2H), 7.25(s, 2H), 4.28(d, *J*=6.6 Hz, 2H), 4.19(s, 1H), 3.79(s, 2H), 2.95(s, 4H), 1.66(s, 4H), 1.45—1.08(m, 8H). IR(KBr), $\tilde{\nu}$/cm^{-1}: 3293, 3192, 3061, 2931, 2859, 1678, 1527, 1425, 1324, 1236, 1171. ESI-TOF-MS, *m*/*z*: calcd. for $C_{27}H_{34}N_4O_4$, 478.26; found, 479.26([M+H]$^+$).

2.3 Synthesis of Fmoc-cyclo(*L*-Lys-*L*-Lys)-Boc(3)

Compound **2**(0.479 g, 1.0 mmol) was dissolved in 16 mL of triethylamine(TEA)/CH_3OH(1:7, volume ratio), and the solution was slowly added to the solution of $(Boc)_2O$(1.5 mmol, 0.327 g) in methanol at 0 °C. The mixture was warmed to room temperature and stirred overnight. Finally it was concentrated, washed with water, and freeze-dried, giving a white solid. Yield: 87%; m. p. 186 °C; ^{1}H NMR(400 MHz, DMSO-d_6, 25 °C), δ: 8.12(s, 2H), 7.86(d, *J*=16.9 Hz, 2H), 7.68(s, 2H), 7.41(s, 2H), 7.33(s, 2H), 6.78(s, 1H), 6.28(s, 1H), 4.28(s, 2H), 4.18(d, *J*=26.2 Hz, 1H,), 3.79(s, 2H,), 2.94(d, *J*=19.5 Hz, 2H), 2.88(s, 2H), 1.64(s, 4H), 1.36(s, 17H). IR(KBr), $\tilde{\nu}$/cm^{-1}: 3337, 3206, 3061, 2938, 1664, 1527, 1447, 1244, 1165. ESI-TOF MS, *m*/*z*: calcd. for $C_{32}H_{42}N_4O_6$, 578.31; found: 579.32([M+H]$^+$).

2.4 Synthesis of Boc-cyclo(*L*-Lys-*L*-Lys)-NH_2(4)

Compound **3**(0.578 g, 1.0 mmol) was dissolved in 20 mL of piperidine/DMF(1:4, volume ratio) for 3 h at 60 °C. The mixture was added in 200 mL of ether, and the precipitate was dried in a vacuum oven. The crude product was dissolved in water to remove a small amount of insoluble substance. The filtrate was freeze-dried. Yield: 87%; m. p. 157 °C; ^{1}H NMR (400 MHz, DMSO-d_6, 25 °C), δ: 8.04(dd, *J*=40.7, 10.8 Hz, 2 H), 6.75(s, 1 H), 3.78(s, 2H), 2.88(d, *J*=5.5 Hz, 4H), 1.64(s, 4H), 1.41—1.18(m, 17H). IR(KBr), $\tilde{\nu}$/cm^{-1}: 3350, 3221, 2990, 1678, 1519, 1439, 1273, 1200, 1012. ESI-TOF MS, *m*/*z*: calcd. for $C_{17}H_{32}N_4O_4$, 356.24; found: 357.25([M+H]$^+$).

2.5 Gelation Tests

A weighed amount of potential gelator and the organic solvent were added to a sealed glass vial to make a total of 1 g of the mixture and heated to get a clear solution. The solution was then cooled back to room temperature in air. The gelation(G) was confirmed by inverting the glass vial and the solution inside the vial showed no evidence to flow. Systems in which only solution remained until the end of the tests were referred as soluble(S) and the precipitates were formed as precipitation(P).

3 Results and Discussion

3.1 Synthesis

The preparative pathway of Fmoc and Boc mono-substituted cyclo(*L*-Lys-*L*-Lys)s is outlined in Scheme 1. Fmoc mono-substituted cyclo(*L*-Lys-*L*-Lys)(**2**) was prepared with lysine cyclic dipeptide(**1**) as starting material to react with Fmoc-OSu under strict control of the molar feed ratio for the sake of facile separation of the target product. Thereafter,

compound **2** further reacted with $(Boc)_2O$ to produce both Fmoc and Boc mono-substituted cyclo(*L*-Lys-*L*-Lys)(**3**). However, as for Boc mono-substituted cyclo(*L*-Lys-*L*-Lys)(**4**), it was not directly obtained from the reaction of compound **1** with $(Boc)_2O$, instead, was generated from the deprotection of compound **3** in a piperidine/DMF mixed solution. The structures of the three lysine cyclic dipeptide derivatives were determined by means of ^{1}H NMR, IR and ESI-TOF MS analyses in this study.

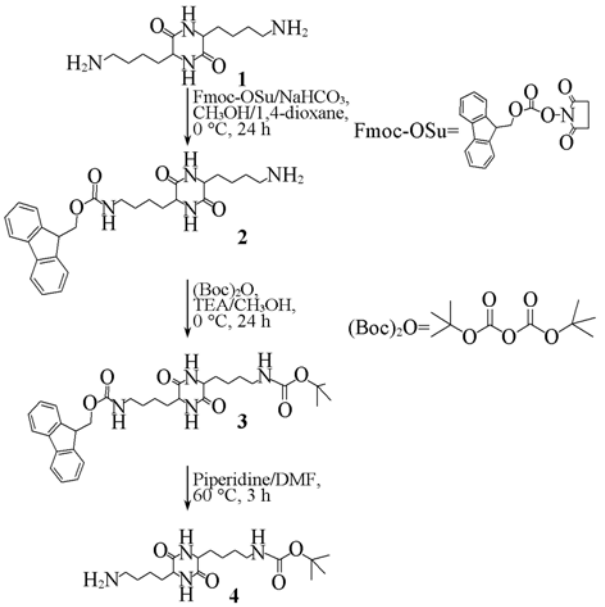

Scheme 1 Synthetic pathway of Fmoc or Boc mono-substituted cyclo(*L*-Lys-*L*-Lys)s

3.2 Gelation Performances

The gelation abilities of compounds **2**, **3** and **4** were evaluated by test tube inversion method, with the results summarized in Table 1. The values in the parenthesis denote MGC data(mass fraction,%) required to gelate a selected solvent at room temperature.

Aiming at preparing unique hydrogelators from lysine cyclic dipeptides, the solubility of Fmoc and Boc mono-substituted compounds **2** and **4** was firstly tested. Compound **4** was found to be soluble in water, showing no gelation even increasing the concentration. However, compound **2** is slightly soluble in water under heating and can form unstable partial hydrogel upon cooling a suspension of 5%(mass fraction) of it to room temperature as shown in Fig.1. It should be noted that the TEM image of compound **2** was taken to observe the self-assembled fibrillar supramolecular polymeric structure at a concentration(mass fraction) of 0.2% instead of 5% in water. As can be seen, compound **2** is self-assembled into nano-fibrillar ribbons, but cannot be further self-aggregated into the 3D fixed fibrillar network to absorb an enormous amount of water to form hydrogel at a concentration of 5%. Moreover, both Fmoc and Boc disubstituted lysine cyclic dipeptide **3** is insoluble in water due to its high hydrophobicity compared with those of compounds **2** and **4**. In view of the fact that compound **2** is slightly soluble, compound **3** fully insoluble and compound **4** well soluble in water, it is expected that a series of hydrogelators could be obtained *via* modifying the exposed amino group in Fmoc or Boc mono-substituted cyclo(*L*-Lys-*L*-Lys)s and mediating the hydrophilic-hydrophobic balance of these LMWGs with alkyl acryl chains, which is our ongoing study.

Table 1 Testing results of gelation behavior and MGC(mass fraction, %, in parenthesis) of gelators toward solvents given by test tube inversion method*

Solvent	Compound **2**	Compound **3**	Compound **4**
DMF	S	S	S
DMSO	S	S	S
THF	PG	I	I
H_2O	PG	I	S
Ethyl acetate	I	G(3%)	I
Dichloromethane	G(3%)	PG	P
Chloroform	G(4%)	S	P
1,2-Dichloroethane	G(3%)	G(2%)	G(3%)
1,1,2,2-Tetrachloroethane	G(3%)	S	G(3%)
Benzene	G(3%)	G(2%)	G(3%)
Methylbenzene	PG	G(2%)	G(3%)
Dimethylbenzene	S	G(2%)	G(3%)
Paraxylene	PG	G(2%)	G(3%)
o-Dichlorobenzene	G(4%)	G(1%)	G(4%)
Methanol	S	I	P
Ethanol	G(3%)	I	P
Isopropanol	G(3%)	PG	P
Butanol	G(3%)	I	P
Hexanol	G(3%)	G(2%)	P
Acetonitrile	G(3%)	S	S

* G: gel; PG: partial gelation; I: insoluble upon heating; S: solution; P: precipitation.

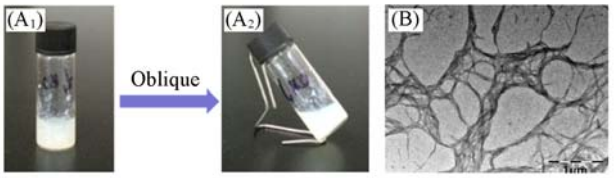

Fig.1 Appearances(A_1—A_2) of partial hydrogel formed by gelator 2(5%) and TEM image(B) of hydrogel fomed from gelator 2(0.2%)

As organogelators, compounds **2**, **3** and **4** are soluble in DMF and DMSO, but can gelate a number of selected organic solvents to yield organogels, depending on the substituting group types and selected solvents. Compared with aliphatic Boc, aromatic Fmoc assists and facilitates the self-assembly of a great number of LMWGs to form gels through the π-π stacking interaction. For example, the promotion of Fmoc to the gelation has been well documented in a series of di- and poly-peptide derivatives[4,5,24,25]. Although Fmoc mono-substituted organogelator **2** cannot form stable hydrogel in water, it can gain access to a series of stable opaque, translucent and transparent organogels in most alcoholic, *o*-dichlorobenzene and chlorinated solvents with MGC kept in a range of 3%—4%. The appearances of organogels formed from organogelator **2** in organic solvents are shown in Fig.2 and the gelation behaviors and MGC data are summarized in Table 1.

The hydrogen bonding interaction between lysine cyclic dipeptides is deemed the main driving force for Boc mono-substituted organogelator **4** to gelate organic solvents.

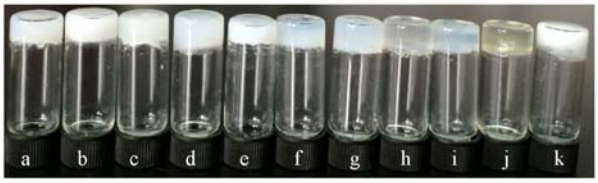

Fig.2 Appearances of organogels formed from organogelator 2 in organic solvents

a. 3%(MGC) in ethanol; b. 3% in isopropanol; c. 3% in butanol; d. 3% in hexanol; e. 3% in dichlormethane; f. 4% in chloroform; g. 4% in 1,2-dichloroethane; h. 3% in 1,1,2,2-tetrachloroethane; i. 3% in benzene; j. 3% in *o*-dichlorobenzene; k. 3% in acetonitrile.

Although it is well dissolved in water, DMF and DMSO, organogelator **4** can gelate the selected substituted benzenes and two of chlorinated solvents to create stable organogels. The appearances of organogels obtained from organogelator **4** are depicted in Fig.3. However, in almost all the alcohols, it becomes soluble under heating, but precipitates when cooled in air. The results suggest that besides the hydrogen bonding interaction, the solubility of lysine cyclic dipeptide served as an LMWG in selected solvents also plays a crucial role in the self-assembly into the fixed 3D fibrillar network to absorb solvents, gaining access to organogels.

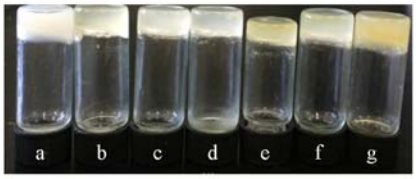

Fig.3 Appearances of organogels formed from organogelator 4 in organic solvents

a. 3%(MGC) in 1,2-dichloroethane; b. 3% in 1,1,2,2-tetrachloroethane; c. 3% in benzene; d. 3% in methylbenzene; e. 3% in dimethylbenzene; f. 3% in paraxylene; g. 4% in *o*-dichlorobenzene.

As shown in Table 1 and Fig.4, the gelation ability of both Fmoc and Boc substituted organogelator **3** is clearly promoted by the cooperative interactions of Fmoc and Boc substituting groups. It gelates not only ethyl acetate, 1,2-dichloroethane and aromatic solvents with MGC in a range of 1%—2% compared with organogelators **2** and **4**, but also hexanol with an MGC of 2% and isopropanol to form partial organogel. The appearances of the resulting stable organogels are similar to those of the organogels formed from organogelator **2** in organic solvents. The results clearly imply the synergic interactions of the π-π stacking and hydrogen bonding in both Fmoc and Boc disubstituted cyclo(*L*-Lys-*L*-Lys).

Like most organogels[11,16,17,26], all the gels obtained from organogelators **2**, **3** and **4** in selected organic solvents are thermal reversible, which can be changed into transparent solutions under heating and gels again under cooling many times.

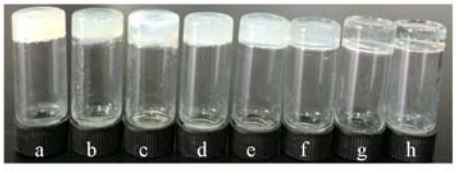

Fig.4 Appearances of organogels formed from organogelator 3 in organic solvents

a. 2%(MGC) in 1,2-dichloroethane; b. 2% in hexanol; c. 2% in ethyl acetate; d. 2% in benzene; e. 2% in methylbenzene; f. 2% in dimethylbenzene; g. 2% in paraxylene; h. 2% in *o*-dichlorobenzene.

3.3 Rheological Measurements

As organogelators **2**, **3** and **4** can form stable organogels in 1,2-dichloroethane, these samples were used to monitor their rheological behavior. The viscoelasticities were characterized by the dynamic storage modulus(G') and the loss modulus(G'') in the oscillatory experiments. Before conducting the strain-controlled analyses, the linear viscoelastic regime of deformations and yield strain of the organogels were first determined by a strain-sweep experiment. The linear regime is that both the dynamic storage and loss moduli are independent of the strain amplitude and reflect the properties of the unperturbed network. As can be seen in the insets of Fig.5, the flowing response of the samples to an ascending strain ramp is revealed by the curve of the dependence of G' on the applied oscillatory strain. As the G' value exhibits a rough plateau in a low strain range, γ_0 is restricted to a low strain of 0.1% as described below with a limit of linearity.

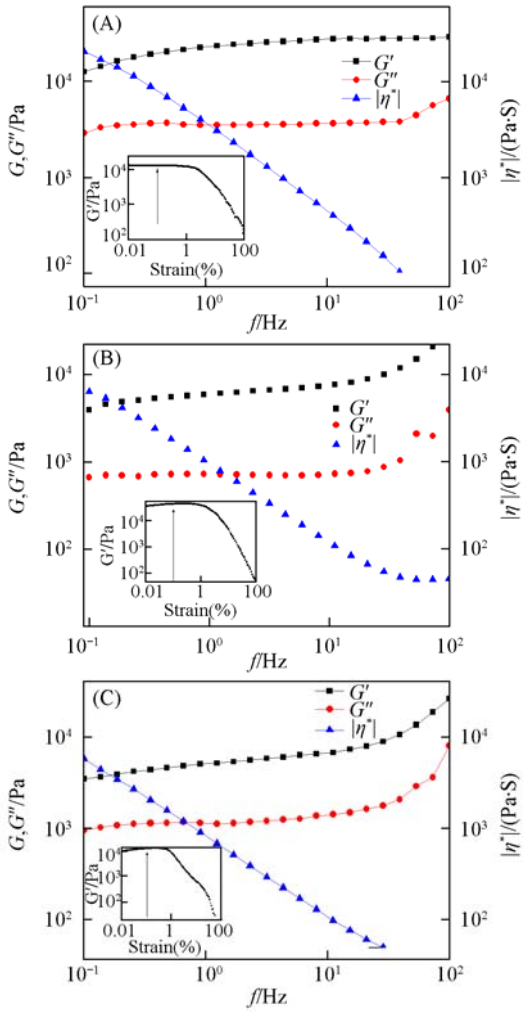

Fig.5 Viscoelastic properties of organogelators 2(A), 3(B) and 4(C) in 1,2-dichloroethane

Mass fraction of organogelators(%): (A) 3; (B) 2; (C) 3. Inset: variation of the elastic shear modulus of the organogels as a function of the applied strain at 25 °C(f=1 Hz).

Fig.5 presents the variation of the dynamic moduli and complex viscosity as a function of the oscillatory frequency. For the three samples, their dynamic storage modulus values stand greater than the loss ones at all frequencies, showing the dominant elastic character of the soft material.

Compared to those of other two samples, the G' value of organogelator **2**(1.3×10^4 Pa) at an oscillatory frequency of 1 Hz is higher than those of organogelator **3**(3.8×10^3 Pa) and organogelator **4**(3.5×10^3 Pa), indicating better mechanical properties of the organogel formed from organogelator **2**. Moreover, the G' values of organogelators **3** and **4** exhibit upturning in a high frequency range, suggesting that the gelator molecules rearranged slowly with the increase of oscillatory frequency. The complex viscosity [η^*] decays linearly at log coordinates. Such a mechanical behavior is such a characteristic of soft viscoelastic solids that these gel samples can be qualified to be organogels[27,28].

3.4 Morphology Observations

During the gelation process, gelator molecules are first self-assembled into nanoscale superstructures, such as nanofibers, nanoribbons, nanotubes and nanosheets[29—32]. The assemblies are then further aggregated into a 3D supramolecular polymeric network to entrap a huge amount of solvent molecules into the network, forming hydro- and organo-gels. To have a visual insight into the morphologies and shapes of these self-aggregates, we carried out the SEM and TEM observations with results illustrated in Figs.6—8, respectively.

The TEM images of the xerogels obtained from organogelator **2** in various alcoholic solvents are shown in Fig.6(A)—(D). These self-assemblies are spiny spherical with an average diameter of up to 0.5—1 μm, which are further entangled with each other through the peripheral "tentacles", representing a cross-linked gel network node and being non-transparent. Accordingly, the spherical aggregates consisting of fiber structure pack can be also observed clearly in the SEM images. The diameter of the aggregates is larger in hexanol than in ethanol, mainly because of the different boiling points of alcoholic solvents. Liu *et al*.[33] introduced an effective method to measure *in-situ* the spherical fractal growth of the fibrous networks of supramolecular materials. They found that at higher cooling rates, the fibers are less linear and coincide with a higher degree of branching. Therefore, when the samples are heated to nearly the boiling point, compound **2** is dissolved in the solvents; and then cooled to room temperature to form organogels. The higher the boiling point is and the larger the cooling rate gets, the higher the degree of branching and hence the bigger spherical aggregates are. It is concluded that with the extending of alkyl chain in aliphatic alcohols, the boiling point of the solvent gets higher gradually, and the cooling rate increases progressively in the same environment, as a result, yielding the greater degree of branching, which impacts the size of the self-assemblies.

At the same time, organogelator **2** in 1,2-dichloroethane [Fig.6(E), (E′)] creates dendritic aggregates about 100—150 nm in width, which are crosslinked loosely with each other to form a 3D network. However, as can be seen from Fig.6(F)—(G) and (F′)—(G′), organogelator **2** is mainly self-assembled into thin and long fibers with a diameter of about 50—100 nm and up to several micrometers in length, and further interwoven into a 3D network in aromatic solvents. Compared to the gels formed in alcoholic solvents, the gels formed in aromatic solvents are more transparent. The self-aggregates are likely to give access to various nano-sized geometries, which result in

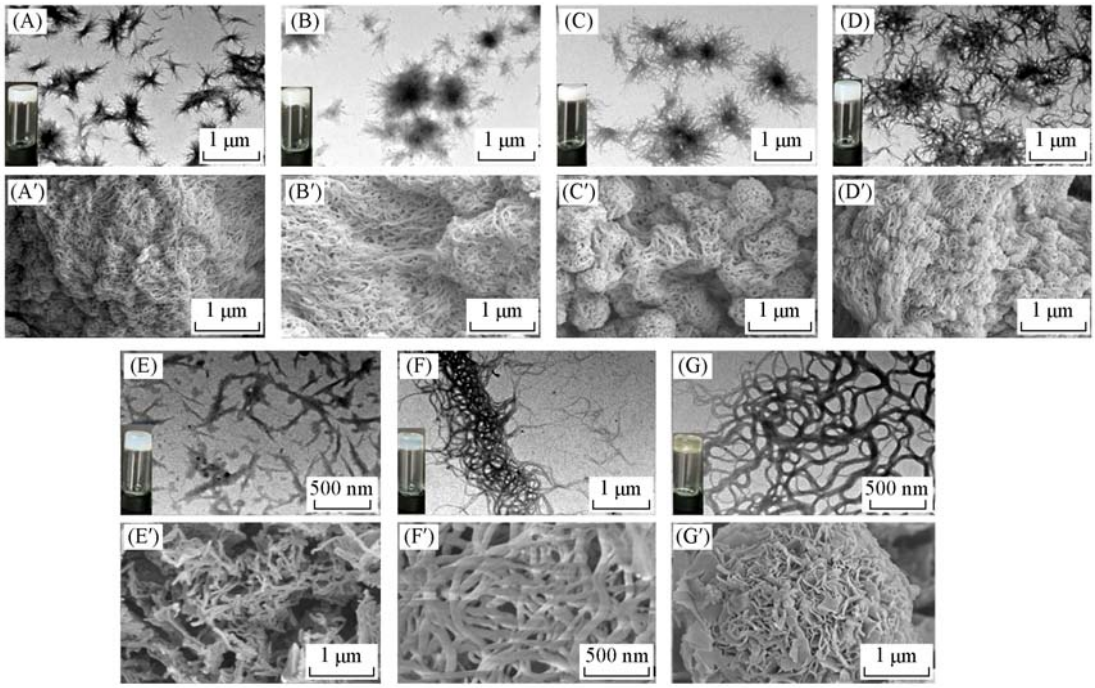

Fig.6 TEM(A—G) and SEM(A′—G′) images of organogels obtained from organogelator 2 in different solvent

(A, A′) Ethanol; (B, B′) isopropanol; (C, C′) butanol; (D, D′) hexanol; (E, E′) 1,2-dichloroethane; (F, F′) benzene; (G, G′) *o*-dichlorobenzene. Insets of (A—G): appearances of organogels formed from organogelator **2** in organic solvents.

different appearances of organogels in different solvents. Therefore, the thinner the fiber diameter is, the more transparent the organogel becomes.

Fig.7 reflects the TEM and SEM images of the organogels formed from organogelator **3** in hexanol, 1,2-dichloroethane and selected aromatic solvents. The organogel prepared in hexanol after freeze-drying possesses a clusters-like geometry with a diameter of 100—250 nm, which is similar to that of fibers of organogelator **2** in alcoholic solvents. Alcoholic solvents affect the self-assembly processes *via* competing the hydrogen bonding interaction with gelators so that the aggregates grow in a multi-dimension mode with the shorter lengths as shown in Fig.6(A)—(D), (A′)—(D′) and Fig.7(A), (A′). In contrast, the organogels formed in 1,2-dichloroethane[Fig.7(B) and (B′)] and substituted benzenes[Fig.7(C)—(F) and (C′)—(F′)] all present a one-dimensional self-assembly to give the uniform and slender entangled nanofiber network with fibrillar geometry. Bundle formations and collapses/shrinkages of the network were also noticed. Especially, the aromatic solvents facilitate organoglater **3** to aggregate into well-developed nanofibers with the diameters of around 20—50 nm. So the organogels fabricated in these solvents display the translucent and transparent appearances. Different from organogelators **2** and **3**, Boc mono-substituted organogelator **4** is self-assembled into organic nanotubes with the inner diameters(i.d.) of 10—100 nm in 1,2-dichloroethane and four substituted benzenes as portrayed in Fig.8. The wall thickness of the self-assembled nanotubes is about 10—20 nm. These nanotubes are overlapped with each other to create the 3D supramolecular polymeric network entrapping selected organic solvents to produce organogels. More interestingly, the obtained self-organized nanotube structures would have the advantage of providing a 1D and confined liquid nanospace under ambient conditions that cannot be produced by microfabrication technology with the great potential to be employed as delivery vehicles in the field of microencapsulation technique and biomedical engineering. For example, these self-organized nanotube structures could store proteins in their nanochannels with controllable diameters and inner surfaces *via* the electrostatic interaction. Shimizu *et al*.[34] reported that organic nanotubes prepared by self-assembling the mono-layer lipid membranes(MLMs) from wedge-shaped bolaamphiphiles with an amino head group can encapsulate myoglobin in the channels of nanotubes and retain its oxygen-binding activity at high concentrations of denaturants.

Furthermore, it was found that the junctions of fibers are usually classified into two types, one is the transient entanglement of fibers, such as Fig.8(A), (A′), (C)—(F) and (C′)—(F′), the cross-cover of the nanotubes without entangling formed by organogelator **4**; and the other is the permanent side- and tip-branching of fibers. These fibrous networks with permanent interconnections will effectively entrap and immobilize solvent molecules in the meshes. Therefore, if the junctions are permanent, the strength of the network is normally higher than that of the network formed by transient junctions[33].

As shown in Fig.6(A)—(E), (A′)—(E′) and Fig.7, most of the fibers are side-branched or tip-branched, and the fibers are entangled together closely instead of simple cross-cover. With the results of rheological test considered, the G' value of organogelator **4**(3.5×10^3 Pa) at a oscillatory frequency of 1 Hz is lower than those of organogelators **2**(1.3×10^4 Pa) and **3**(3.8×10^3 Pa) , so that the better mechanical properties of organogels can be and have been obtained from organogelators **2** and **3**.

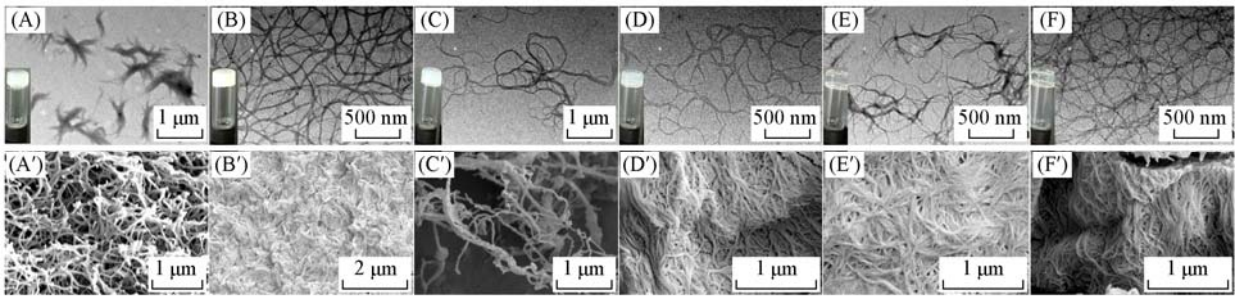

Fig.7 TEM(A—F) and SEM(A′—F′) images of organogels obtained from organogelator 3

(A, A′) Hexanol; (B, B′) 1,2-dichloroethane; (C, C′) methylbenzene; (D, D′) dimethylbenzene; (E, E′) paraxylene; (F, F′) *o*-dichlorobenzene. Inset: appearances of organogels formed from organogelator **3** in organic solvents.

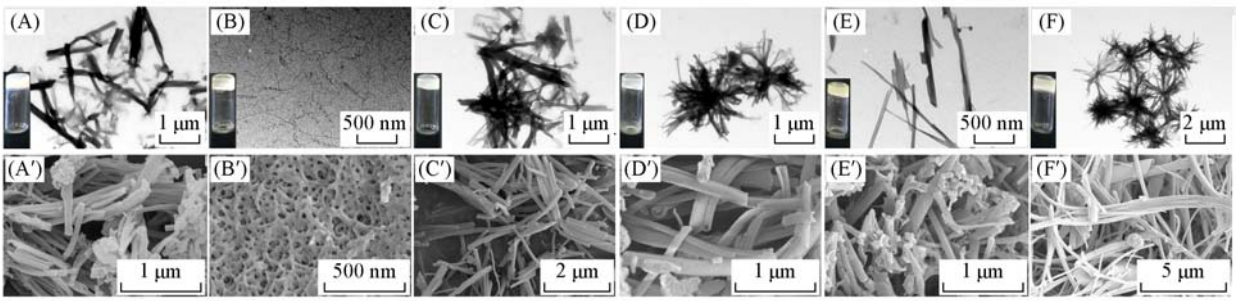

Fig.8 TEM(A—F) and SEM(A′—F′) images of organogels obtained from organogelator 4

(A, A′) 1,2-Dichloroethane; (B, B′) 1,1,2,2-tetrachloroethane; (C, C′) benzene; (D, D′) methylbenzene; (E, E′) dimethylbenzene; (F, F′) paraxylene. Inset: appearances of organogels formed from organogelator **4** in organic solvents.

3.5 Driving Forces for Self-assembly

Since both organogelators **2** and **3** contain Fmoc groups having a big π-conjugated structure, the π-π stacking interactions between the gelator molecules should be one of the most important driving forces for their self-assembly into the 3D supramolecular polymeric network in most organic solvents. Consequently, the fluorescence spectrum was measured to highlight the arrangement of fluorenyl groups in solutions and organogels. The results are depicted in Figs.9 and 10, respectively.

As shown in Fig.9, organogelator **2** in 1,2-dichloroethane and benzene exhibits very similar emission spectra with two emission peaks centered at 320 and 460 nm nearby. The peak at 320 nm, as the emission peak of Fmoc group, is red-shifted slightly to 324 nm with increasing the concentration due to the π-π stacking interaction. The intensity of this peak is decreased gradually while the intensity of emission peak at 460 nm is markedly enhanced as a function of concentration(0.125%—3%). This is a characteristic excimer emission of the Fmoc-group with the J-type aggregation which is an indication of strong intermolecular π-π interaction[35]. This type of aggregates was also observed previously in the literature[15—17,36].

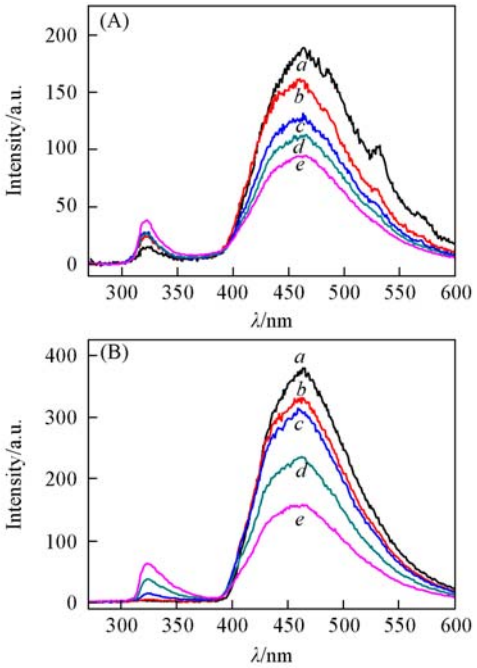

Fig.9 Fluorescence emission spectra of organogelator 2 in 1,2-dichloroethane(A) and benzene(B)

λ_{ex}=265 nm. (A) *a*. 3% gel; *b*. 1% solution; *c*. 0.5%; *d*. 0.25%; *e*. 0.125%. (B) *a*. 3% gel; *b*. 1% solution; *c*. 0.5% solution; *d*. 0.25% solution; *e*. 0.125% solution.

As seen in Fig.10(A), the fluorescence spectrum of organogelator **3** in 1,2-dichloroethane displays the emission peak of Fmoc group shifted from 317 nm to 333 nm with increasing the concentration from 0.125% to 2%. Meanwhile, there is nearly no peak visible at 460 nm as a function of concentration. The obvious red shift of fluorenyl groups in the gels indicates that the fluorenyl groups are stacked more extensively in the organogel. However, its fluorescence spectrum in *o*-dichloroben- zene is similar to that of organogelator **2** in benzene as depicted in Fig.10(B). The emission peak of Fmoc groups is red-shifted from 324 nm to 331 nm, and a broad and increased phosphorescence peak appears at 460 nm with the increase of concentration(0.125%—1%). It suggests that the fluorenyl groups are overlapped more efficiently and there is an extensive J-aggregate manner in benzene solvent. Although the morphologies of the organogels obtained from organogelator **3** in 1,2-dichloroethane and *o*-dichlorobenzene look similar as shown in Fig.7, their fluorescence emission spectra are quite different, indicating the different stacking structures in different solvents. In *o*-dichlorobenzene, the solvent molecules may interact with the Fmoc group of the gelator *via* π-π stacking interactions so that the stacking of Fmoc groups in *o*-dichlorobenzene differs from that of those in 1,2-dichloroethane.

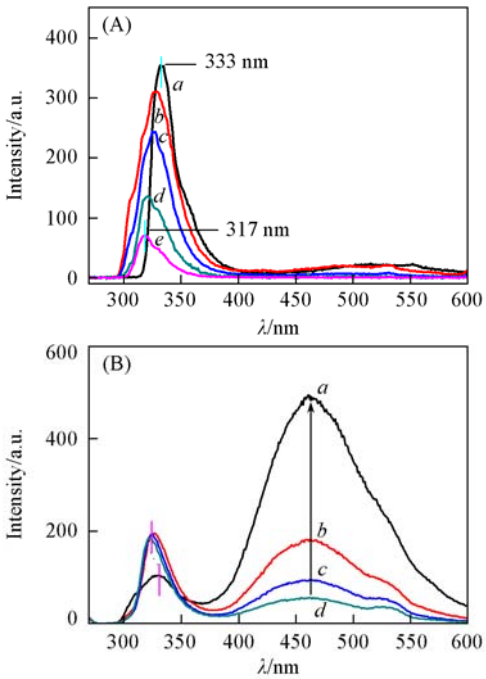

Fig.10 Fluorescence emission spectra of organogelator 3 in 1,2-dichloroethane(A) and *o*-dichlorobenzene(B)

λ_{ex}=265 nm. (A) *a*. 2% organogel; *b*. 1%; *c*. 0.5%; *d*. 0.25%; *e*. 0.125%. (B) *a*. 1% organogel; *b*. 0.5% solution; *c*. 0.25% solution; *d*. 0.125% solution.

As the hydrogen bonding interaction among lysine cyclic dipeptide moleculars is the main driving force for organogelator **4** to self-assemble in organic solvents, the FTIR spectra were measured to check the influence of hydrogen bonding interaction on its gelation process. As shown in Fig.11 curve *a*, the peak at 3457 cm^{-1} is ascribed to the stretching vibration absorption of free N—H bonds of amide groups and the other two peaks at 1675 and 1515 cm^{-1} are assigned to the stretching vibration absorption of free amide I and bending vibration absorption of free amide II due to the gelator well dissolved in DMSO. However, the N—H stretching vibration peak is red-shifted to 3350 cm^{-1} and those of amide II are blue-shifted to 1520—1525 cm^{-1} in the gels formed from organogelator **4** in benzene and methylbenzene(Fig.11 curvese *b* and *c*). Meanwhile this peak becomes wider when amide II is in the solid

state(Fig.11 curve *d*). This offers evidence to support the hydrogen bonding interaction as the main driving force to promote organogelator **4** self-assembling into the 3D fibrillar supramolecular polymeric network to entrap a huge amount of solvent molecules to form the organogels.

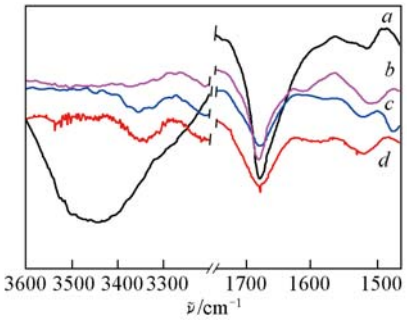

Fig.11 IR spectra of organogelator 4

a. Solution in DMSO; *b*. organogel in methylbenzene; *c*. organogel in benzene; *d*. organogelator in solid state.

The FTIR spectra of organogelator **3** are showed in Fig.12. As seen, the peak of the stretching vibration absorption of free N—H bonds of amide groups is red-shifted from 3430 cm^{-1} to 3350 cm^{-1} with it changing from the free state in DMSO(Fig.12 curve *e*) into the gels(Fig.12 curves *b*, *c* and *d*), and this peak is further red-shifted to 3310 cm^{-1} in the solid state(Fig.12 curve *a*). Combined with the fluorescence spectra of organogelators **2** and **3**, the results demonstrate that the cooperation of the hydrogen bonding interaction of amide linkage with π-π stacking interaction of Fmoc groups makes a contribution to the self-assembly processes of Fmoc mono-substituted cyclo (*L*-Lys-*L*-Lys).

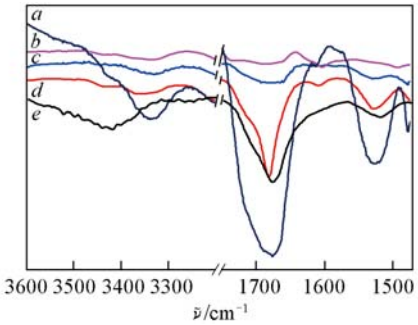

Fig.12 IR spectra of organogelator 3 in different states

a. Solid state; *b*. in methylbenzene; *c*. in benzene; *d*. in 1,2-dichloroethane; *e*. in DMSO.

3.6 Simulation of Molecular Configuration

Powder X-ray diffraction is a powerful tool to deduce and determine the possible packing structure of gelators at the molecular level. As only wide dispersing diffraction peaks appear in the XRD patterns of xerogels from organogelators **2** and **3**, it is difficult to simulate their possible packing structures. Fortunately, a series of high-resolution XRD patterns of xerogel **4** was obtained with strong well-resolved diffraction peaks. The patterns are illustrated in Fig.13.

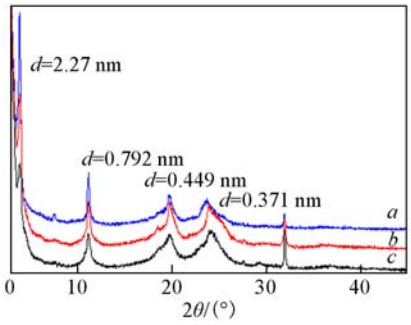

Fig.13 XRD patterns of xerogel prepared from organogelator 4 in dimethylbenzene(*a*), benzene(*b*) and 1,2-dichloroethane(*c*)

In comparison to the out-of-order molecular arrangement of organogelators **2** and **3**, that of exrogel from organogelator **4** is resulted from its self-assembly into nanotubes in 1,2-dichloroethane and substituted benzenes as mentioned above. As can be seen, although the thicknesses of these nanotubes are varied in a range of 10—20 nm, their XRD patterns of the xerogels of organogelator **4** formed in 1,2-dichloroethane, benzene and dimethylbenzene are similar in the diffraction peak positions. A primary reflection peak was found in the low 2θ angle region, corresponding to d=2.27 nm, or to the wall thickness of BLM structure. Meanwhile, a characteristic diffraction peak of β-sheet arrangement corresponds to d=0.449 nm. It suggests that the gelator **4** possesses the same arrangement pattern of self-assemblies in these three solvents. Noteworthily the formation of nanotubes from the chiral amphiphiles, referred to as "chiral self-assembly", often occurs with mono polar amphiphiles possessing a single head group and single or double tails. For example, some amphiphiles generate nanotubes in a way to construct BLM structures from hot aqueous solutions upon their cooling[37].

As a hydrophobic substituting group, the Boc group in organogelator **4** should form the outer hydrophobic part in hydrophobic solvents as it directly interacts with solvent molecules. The amino-terminals of organogelator **4** should interact with each other *via* the hydrogen bonding interaction. The DKP skeletons and the amides of the side chains of organogelator **4** are held together by the strong intermolecular hydrogen bonding interactions. As shown in Fig.14, the wall thickness of the

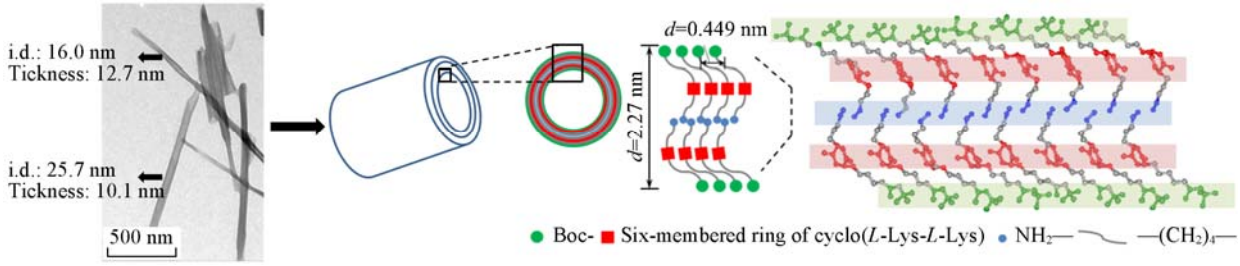

Fig.14 Schematic images of self-assembled nanotubes obtained from organogelator 4 in dimethylbenzene within the solid bilayer membranes

nanotubes obtained in dimethylbenzene is over 10 nm, thus it is concluded that the self-assembled nanotubes are stacking of multiple BLMs[34,38]. Interestingly, the bigger the inner diameter is, the thinner the thickness becomes. This is because the interactions between bilayer membranes get weaken when the i.d. becomes larger, so the number of bilayer membranes needed is decreased. For instance, when the wall thickness of the self-assembled nanotubes is 10.1 nm, four BLMs are needed to be stacked together to form the 1D hollow cylinder. Moreover, when the i.d. is 16.0 nm, five BLMs are required.

4 Conclusions

Three obtained Fmoc and Boc mono-substituted cyclo(*L*-Lys-*L*-Lys)s enable to gelate most selected alcoholic, substituted benzene and chlorinated solvents. These organogelators are self-assembled into 3D nanofiber, nanoribbon or nanotube network structures. The π-π stacking interactions play the main driving force to promote Fmoc mono-substituted organogelator **2** to self-assemble into the fibrillar polymeric network, while the hydrogen bonding interactions act as the main driving force to benefit organogelator **4** self-assembling into the nanotube polymeric network. The XRD patterns obtained from the nanotubes of organogelator **4** help to infer the stacking of multiple BLMs. The nanotubes with a well-defined hollow cylindrical morphology show the potential to be used in the area of microencapsulation technique and biomedical engineering.

References

[1] Steed J. W., *Chem. Commun.*, **2011**, *47*, 1379

[2] Suzaki Y., Taira T., Osakada K., *J. Mater. Chem.*, **2011**, *21*, 930

[3] Hanabusa K., Suzuki M., *Polym. J.*, **2014**, *46*, 776

[4] Yang Z., Gu H., Zhang Y., Wang L., Xu B., *Chem. Commun.*, **2004**, 208

[5] Zhang Y., Gu H., Yang Z., Xu B., *J. Am. Chem. Soc.*, **2003**, *125*, 13680

[6] Borthwick A. D., *Chem. Rev.*, **2012**, *112*, 3641

[7] Marchini M., Mingozzi M., Gennari C., *Chem. Eur. J.*, **2012**, *18*, 6195

[8] Dufour E., Garcia J., *Org. Biomol. Chem.*, **2014**, *12*, 4964

[9] Ou C. W., Wang H. M., Chen M. S., *Chin. J. Chem.*, **2012**, *30*, 1781

[10] Sasaki Y., Akustu Y., Suzuki K., Kisara K., *Chem. Pharm. Bull.*, **1982**, *30*, 4435

[11] Xie Z. G., Zhang A. Y., Ye L., Wang X., Feng Z. .G., *Soft Matter*, **2009**, *5*, 1474

[12] Hanabusa K., Fukui H., Suzuki M., Shirai H., *Langmuir*, **2005**, *21*, 10383

[13] Hoshizawa H., Minemura Y., Yoshikawa K., Suzuki M., Hanabusa K., *Langmuir*, **2013**, *29*, 14666

[14] Xie Z. G., Zhang A. Y., Ye L., Wang X., Feng Z. G., *J. Mater. Chem.*, **2009**, *19*, 6100

[15] Zong Q. Y., Geng H. M., Wang L., Ye L., Zhang A. Y., Feng Z. G., *Acta Chim. Sinica*, **2015**, *73*, 423

[16] Geng H. M., Zong Q. Y., Ye L., Zhang A. Y., Feng Z. G., *Chin. J. Appl. Chem.*, **2015**, *32*, 900

[17] Geng H. M., Zong Q. Y., You J., Ye L., Zhang A. Y., Shao Z. Q., Feng Z. G., *Sci. China Chem.*, **2015**, *59*, 293

[18] Huang Z., Kang S. K., Banno M., Yamaguchi T., Lee D., Seok C., Yashima E., *Science*, **2012**, *337*, 1521

[19] Eisele D. M., Cone C. W., Bloemsma E. A., Vlaming S. M., Rabe J. P., Vanden B. D., *A. Nat. Chem.*, **2012**, *4*, 655

[20] Zhang W., Jin W. S., Fukushima T., Saeki A., Seki S., Aida T., *Science*, **2011**, *334*, 340

[21] Xie Z. G., Zhang A. Y., Ye L., Feng Z. G., *Acta Chim. Sinica*, **2008**, *66*, 2620

[22] Maria A. M., Jordi J. B., *Macromol. Chem. Phys.*, **2006**, *207*, 615

[23] Kaur N., Zhou B., Breitbeil F., Hardy K., Trantcheva I., *Mol. Pharm.*, **2008**, *2*, 294

[24] Raeburn J., Cristina M. C., Adams D. J., *Soft Matter*, **2015**, *11*, 927

[25] Lange S. C., Unsleber J., Wallera P. M., Ravoo B. J., *Org. Biomol. Chem.*, **2015**, *13* 561

[26] Huang R. L., Qi W., Feng L. B., Su R. X., He Z. M., *Soft Matter*, **2011**, *7*, 6222

[27] Fichman G., Manohar S., Guterman T., Seliktar D., Messersmith P. B., Gazit E., *NANO*, **2014**, *8*, 7220

[28] Zhang F. J., Xu Z. H., Dong S. L., Feng L., Song A. X., *Soft Matter*, **2014**, *10*, 4855

[29] Qin S. Y., Wang Q. R., Peng M. Y., Zhang X. Z., *Chin. J. Chem.*, **2014**, *32*, 22

[30] Skilling K. J., Citossi F., Bradshaw T. D., Ashford M., Kellam B., Marlow M., *Soft Matter*, **2014**, *10*, 237

[31] Yang Z. M., Xu B., *J. Mater. Chem.*, **2007**, *17*, 2385

[32] Solsona M. T., Miravet J. F., *Chem. Eur. J.*, **2014**, *20*, 1023

[33] Li J. L., Liu X. Y., *Adv. Funct. Mater.*, **2010**, *20*, 3196

[34] Shimizu T., Minamikawa H., Masuda M., *Polym. J.*, **2014**, *46*, 831

[35] Smith A. M., Williams R. J., Uljin R. V., *Adv. Mater.*, **2008**, *20*, 37

[36] Manchineella S., Govindaraju T., *RSC Adv.*, **2012**, *2*, 5539

[37] Kameta N., Minamikawa H., Masuda M., *Soft Matter*, **2011**, *7*, 4539

[38] Masuda M., Shimizu T., *Langmuir*, **2004**, *20*, 5969